# Hyperspectral Pansharpening Using Principal Component for Samarra City

**Rawnak A. Abdulwahab[1] Laith A. Al-Ani[1] Auday H. Shaban [2]**
[1] Physics Dept., College of Science, Al-Nahrain University, Baghdad/ Iraq.
[2] Department of Remote Sensing, College of Science, University of Baghdad, Baghdad/ Iraq.
E-Mail: Rawnak.rsc@gmail.com

**Abstract**

The hyperspectral imaging is efficiently discriminating between different types of land cover because it utilizes narrow bands of the electromagnetic spectrum. However, the spatial resolution of hyperspectral images might not match their spectral resolution due to certain manufacturing limitation. In order to solve this issue, research was aim of improving the hyperspectral images spatial resolution by using of Principal Component (PC) fusion method. In particular, the research focused on fusing the hyperspectral image which obtained from Hyperion sensor on the Earth Observation one (EO-1) satellite, it has a spatial resolution of (30) meters, with the panchromatic image obtained from the Operational Land Imager (OLI) sensor on the Landsat-8 satellite, which has a high spatial resolution of (15) meters. The research study area located between 395632.4994 - 401212.3000 East and 3789142.5003 - 3780952.6126 North in the Samarra region of Salah Al-Din province. Many preprocessing techniques have been applied on hyperspectral image, involving the elimination of bad bands and bad columns, in addition to the application of radiometric, atmospheric, and geometric corrections. The results were supported by both visual and quantitative assessments of the fusion outcomes for red, green and blue bands. Where blue band shows the highest correlation and the best information.

**Keywords**: Hyperspectral Images, Hyperspectral Remote, Sensing Fusion and Pansharpening.

## زيادة الدقة المكانية للصور الفضائية الفائقة الطيف باستخدام تحليل المركبة الأساسية لمدينة سامراء

**رونق عادل عبد الوهاب[1] ليث عبد العزيز العاني[1] عدي حاتم شعبان[2]**
[1]كلية العلوم /جامعة النهرين، -جامعة النهرين، بغداد/ العراق [2]كلية التحسس النائي /جامعة بغداد-جامعة بغداد، بغداد/ العراق

**الخلاصة**

ان تقنية التصوير الفائق الدقة الطيفية اثبتت كفاءة عالية بقدرته على التمييز بين أنواع الغطاء الأرضي من خلال اعتماده التصوير بحزم ضيقة جدا من الطيف الكهرومغناطيسي. الصور الفائقة الدقة الطيفية تكون دقتها المكانية ضعيفة لمحددات صناعية. للتعامل مع هذه المسألة فان البحث يهدف الى تعزيز الدقة المكانية للصور الفائقة الدقة الطيفية من خلال توحيدها مع صور ذات دقة مكانية اعلى باستخدام تقنية تحليل المركبة الاساسية. ان الصور المستخدمة هي الصور الفائقة الدقة الطيفية الملتقطة من المستشعر Hyperion للقمر الصناعي (EO-1) والتي دقتها المكانية (٣٠ متر) لإنجاز تقنية التوحيد مع صورة panchromatic من المستشعر (OLI) للقمر الصناعي لاندسات-٨ بدقة مكانية (١٥ متر) حيث تقع منطقة الدراسة المختارة لهذا البحث في مدينة سامراء في محافظة صلاح بين401212.3000-395632.4994 شرقا و3789142.5003-3780952.6126 شمالا. ان الصور الفائقة الدقة تضم عدد من الحزم والاعمدة الغير جيدة تبعا لذلك تم استخدام العديد من تقنيات المعالجة المسبقة عليها بما في ذلك إزالة الحزم والاعمدة السيئة، بالإضافة إلى تطبيق التصحيح الإشعاعي والتصحيح الجوي والتصحيح الهندسي. لغرض زيادة الدقة المكانية لصورة الفائقة الدقة الطيفية المعالجة قمنا باعتماد تقنية تحليل المركبة الأساسية. النتائج دعمت من ناحيتين بصريا وكميا باستخدام عدة أنواع من المعايير على ثلاث حزم من الصورة الناتجة. أظهرت الحزمة باللون الأزرق من الطيف المرئي ترابط عالي جدا مع الصورة قبل الدمج إضافة الى احتوائها القدر الأكبر من المعلومات.

**الكلمات المفتاحية:** الصور الفائقة الدقة الطيفية، التحسس النائي الفائق الطيف، زيادة حدة الصور باستخدام أحادية الطيف والتوحيد.

## Introduction

Hyperspectral (HS) images, HS remote sensing data, or HS data cubes are images that collect information across a broad range of wavelengths or spectral bands, often from the visible to the near-infrared or even shortwave infrared portions of the electromagnetic spectrum. Each of the tens to hundreds of spectral bands in HS images offers details about the scene's reflectance or radiance at a specific wavelength. This abundance of spectral data enables accurate characterization of the materials and features found on the Earth's surface because every kind of material has a unique spectral signature that can be used for identification and investigation. *(*Lodhi,*et al.*,2018) (Awad, 2018) Reducing the amount of data, supplying significant features, and producing an image that is more suited for analysis are the three primary objectives of image fusion algorithms (Selva, *et al.*, 2015). (Zihao, *et al.* 2021) proposed a fusion algorithm which consists of two stages, they were image registration and image fusion (Ying, *et al.*, 2021). While (Imani and Ghassemian,2020) tested three general categories by applying spectral spatial fusion models. (Camacho, *et al.*,2022) proposed an HS-MS viewer fusion algorithm based on the spectral unmixing accounting method implemented by the augmented linear mixing model. A new fusion technique by using a non-negative block-term tensor model to estimate HS images with optimal high spatial resolution has been presented by (Guo,*et al.*,2022). (Rawnak., *et al.*2023) fused HS image with PAN using three techniques based on Minimum Noise Fraction, as well as they adopted a new fusion method by using spectral grouping from Principal Component Analysis transform in 2023 (Rawnak, *et al.*, 2023).

## Aim of work

The present work aimed to combine the high spatial resolution of PAN image with high spectral resolution of HS image, and analyze them in an integrated fashion as well as taking advantage of the complementary properties of the two data sources.

| Instrument | Hyperion |
|---|---|
| *Spectral Range* | 0.4 to 2.5 µm |
| *Visible bands* | 35 |
| *NIR bands* | 35 |
| *SWIR bands* | 172 |
| *Spatial resolution* | 30 m |
| *Swath width* | 7.5 km |
| *Spectral coverage* | Continuous |
| *Bandwidth* | 10 nm |
| *Number of bands* | 220 |
| *Temporal resolution* | 200 days |

**Table 1. Hyperion characteristic (Beck, 2003)**

## Remote Sensing Data

The panchromatic (PAN) and HS images used in this research are from Landsat 8 and EO-1 respectively.

Landsat 8 satellite PAN image was taken by the Operational Land Imager (OLI) sensor in date of 18 February 2017 with size 15481 x 15741. The PAN image spatial resolution is (15m) and it covers the wavelength from (0.5 to 0.68 µm). This image was radiometrically and atmospherically corrected using Internal Average Relative Reflectance (IARR) tool which is defined as a calibration technique used to normalize images to the mean range of a scene using ENVI (5.6) software. While, the EO-1 satellite images (EO1H1690362017056110KF_1R) taken by the Hyperion sensor consists of 242 bands. The spatial resolution of this sensor is (30 m) and covers wavelength from (0.356–2.577 µm) with (0.01 µm) intervals. The date of image is on 25 February 2017 and the swath is 256 pixels wide (7.68 km) and (180 km) long. Figure 2 presents the base images used in this research in each OLI and Hyperion of the study area

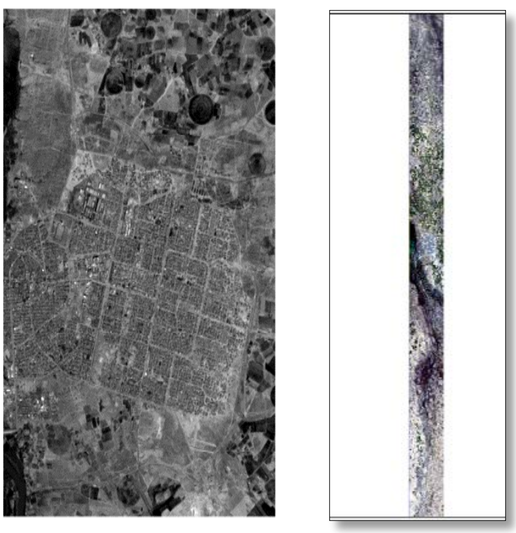

a) OLI -PAN Image

b) EO-1- HS Image (R=22, G=13, B=5)

**Figure 2. The images used in each OLI and Hyperion of the study area.**

### The Study Area

The study area is located in Samarra, Salah Al-Din province. This province is located to the north of Baghdad (Shimal, *et al*., 2020) as shown in Figure 1. This study area scene situation between 395632.4994 - 401212.3000 East and 3789142.5003 - 3780952.6126 North.

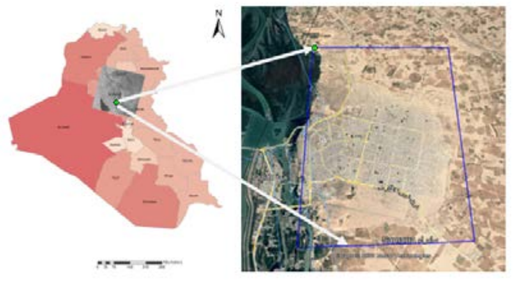

**Figure 1. The study area (Samarra city, Salah al-Din province).**

### Methodology

The methodology has been used in the research divided into two parts:

### Pre-processing of Hyperspectral Images

HS images rely on spectrometer imaging and need to preprocess the raw data to be applicable to analyze the outputs.

### Bad Band Removal

the data product which has been used in this research was level one radiometric (l1r) product**,** this product of hs images contains 242 bands. however, just 198 bands of them contain information and they called non-zero bands. in contrast, the zero bands are specified from one to seven and from 225 to 242. in addition, the bands 58 to 76 which lie in the overlapping region of hyperion which have two spectrometers (spec).

the non-zero bands include two bands with very high noisy due to the overlapped images. they are 77 and 78 and should be eliminated, which left 196 bands (Griffin and Burke, 2003)**.** the rest 196 bands contain the (water vapor) absorption bands which absorbed most of the solar radiation. these bands contain bad information as well as very high noise. the absorption bands can be visually identified and eliminated, and all excluded bands are listed in table 2, which are divided into six groups as shown in figure 3. where image (3a) is a hs in rgb (red, green, blue) color model, image (3b) is one example of first group zero bands (1-7). the second group of zero bands start from band 58 to band 76, (3c) represents band 58. while images from (3d to3i) are examples of noisy bands.

**Table 2. The eliminated bands in the scene [Researcher].**

| No. | The band's number | Band's wavelength (nm) |
|---|---|---|
| 1 | 1-7 | 335 - 416 |
| 2 | 58-70(1st spec) | 935-1075 |
| 3 | 71-78 (2nd spec) | 851 - 922 |
| 4 | 121-126 | 1356 - 1406 |
| 5 | 165-187 | 1800 - 2022 |
| 6 | 191-193 | 2026- 2028 |
| 7 | 2٠٩ and higher | ≥2244 |
| rest | =148 bands | |

## Bad Column Removal

The Hyperion sensor is a push-broom type with two spectrometers visible and near-infrared (VNIR) and short-wave-infrared (SWIR) and it has poorly calibrated in them (un, 2014) . This weakness in calibration leaves errors with high frequencies "bad columns" on the HS bands. The L1R product that used in this research has unaltered column which left to the user. When navigate the HS bands (good bands) scene there are a number of bad dark or white columns in random places within the bands. These columns must correct by replacing them with the average of its neighbors' columns. Figure 4 display some of these columns before removing them.

## Radiometric and Atmospheric Corrections

The satellite sensors either multispectral or hyperspectral captures the data as radiance but records the information as Digital Number (DN). Though, it should be calibrated to

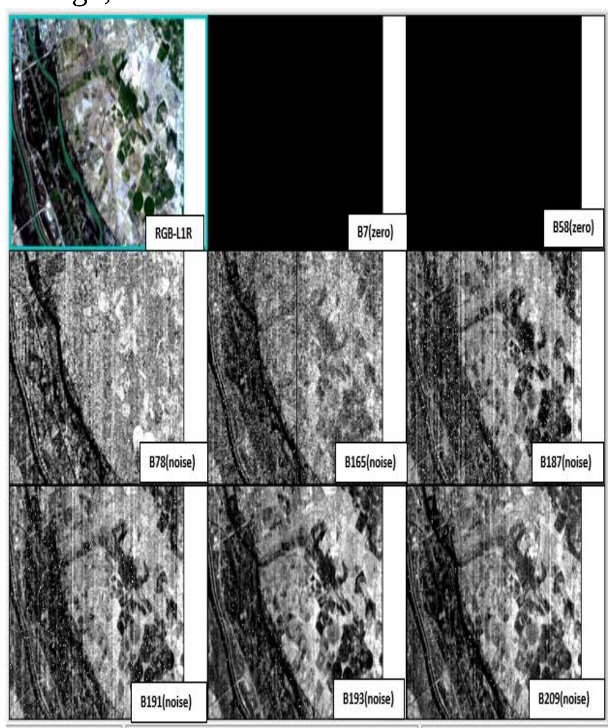


**Figure 3. (a) HS in RGB model (b) and (c) are examples of zero bands. (d) to (i) are examples of noisy bands [Researcher].**

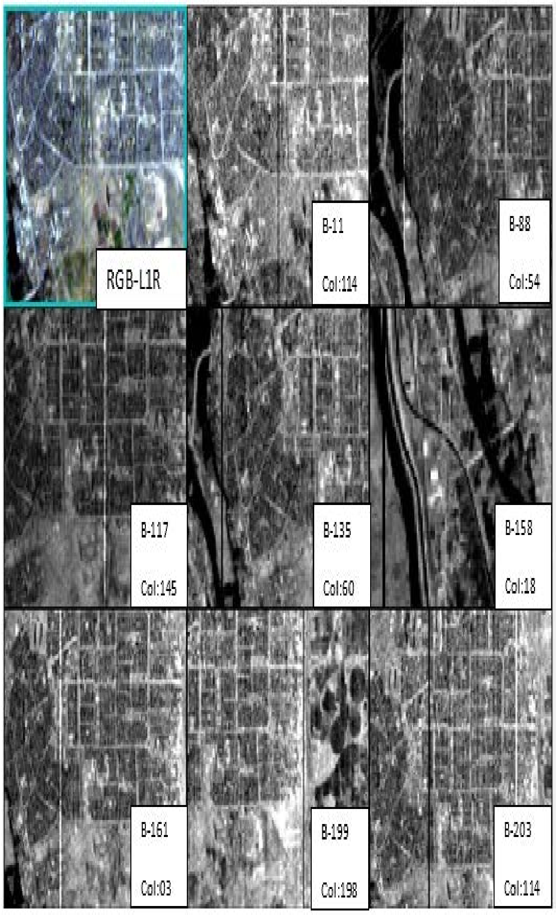


**Figure 4. Review bad columns of HS bands in the scene [Researcher].**

## Geometric Correction

Since L1R products format are not geometry corrected, it will be geometrically corrected. The geometry correction of the HS image was carried out based on the geometry-corrected pan image from the Landsat 8 satellite, and by selecting (25) points manually as ground control points (GCPs) from the two images as shown in Figure 5. The cross-correlation method was used as a matching method based on the Fit Global Transform as the geometric method by first order polynomial and bilinear resampling. In addition, the RMSE has been minimized to 0.25.

**Table3.Parameters used for FLAASH atmospheric correction [researcher].**

| Required Parameter | Value | Ref |
|---|---|---|
| ***Scene Center Location*** | 397682.18 m E<br>3781217.56 m N | HS Meta file |
| ***Sensor Altitude*** | 705 km | HS Meta file |
| ***Ground Elevation*** | 0.065 km | Google earth |
| ***Pixel size*** | 30 m | HS Meta file |
| ***Flight Date*** | 25$^{th}$ Feb 2017 | HS Meta file |
| ***Flight Time*** | 5:18:58(HH:MM: SS) | HS Meta file |
| ***Atmospheric Model*** | MLS | Table appendix A |
| ***Water Retrieval*** | No | Appendix A |
| ***Water Column Multiplier*** | 1.00 | Appendix A |
| ***Aerosol Model*** | Rural | Table appendix A |
| ***Aerosol Retrieval*** | 2- Band (K-T) | Table appendix A |
| ***Initial Visibility*** | 40 km | Table appendix A |
| ***Spectral Polishing*** | Yes | Appendix A |
| ***Width (No. of Bands)*** | 9 | Appendix A |
| ***Wavelength Recalibration*** | No | Appendix A |

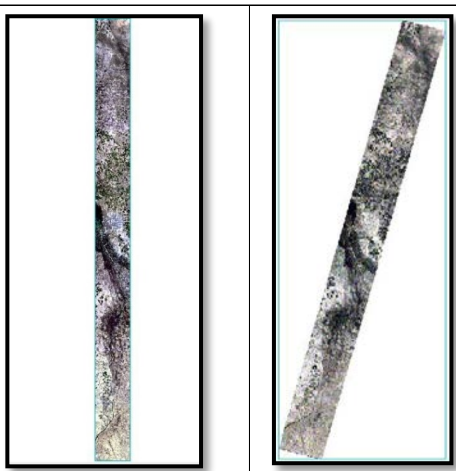

a) HS image before geometric correction | b) HS image after geometric correction

**Figure 5. The HS image before and after geometric correction.**

PAN Image HS image

**Figure6.Reference resized and registered images.**

## Spatial Subset and Image Registration

The study area is subset of both the PAN and HS images in order to fuse them. Map coordinates were used to subset the two images to increase accuracy. These two images were registered together as a preceding step before they were fused (see Figure 5). The RMSE used for registration was less than (0.15).

## Principal Component Analysis (PCA) fusion Technique

PCA is a popular technique used for image fusion specially in remote sensing (Selva, *et al.*, 2015). The theoretical basis for image fusion with PCA lies in the principles of linear algebra and multivariate statistics, and the technique involves extracting the most relevant information from multiple input images using PCA and combining them into a single fused image using a fusion method. PCA is a dimensionality reduction technique that can be used to identify the most important features in a dataset (Jasim, *et al.*, 2018). The PCA is a statistical method based on the eigenvalue decomposition of the covariance matrix ($\mathbf{C_x}$), which takes the form of (Saadallah, 2023):

$$C_x = ADA^T \quad (1)$$

Where: $\mathrm{D} = \mathrm{diag}\,(\lambda_1, \lambda_2, \dots, \lambda_N)$ is the diagonal matrix composed of the eigenvalues $(\lambda_1, \lambda_2, \dots, \lambda_n)$ of the covariance matrix $C_x$, and A is the orthogonal matrix composed of the corresponding N dimension eigenvectors.

$$\boldsymbol{A} = \begin{pmatrix} \boldsymbol{e_{1,1}} & \cdots & \boldsymbol{e_{1N}} \\ \vdots & \ddots & \vdots \\ \boldsymbol{e_{N,1}} & \cdots & \boldsymbol{e_{N,N}} \end{pmatrix} \quad (2)$$

$e_{ij}$ : The $j^{th}$ component of the $i^{th}$ Eigenvector.

The fusion of HS and PAN images can result in a fused image that has both high spectral fidelity and high spatial resolution, which can be beneficial in various applications, such as remote sensing, agriculture, environmental monitoring, and urban planning (Aiazzi, *et al.*, 2007).

This research adopted PC fusion techniques to fuse HS and PAN images. However, the PC fusion rely on CS methodology (Shabin, *et al.*, 2020), thus it replaced the PAN image by first PC then implement the PCA inverse transformation to get fused image. Figure 7 shows the systematic steps of PCA fusion:

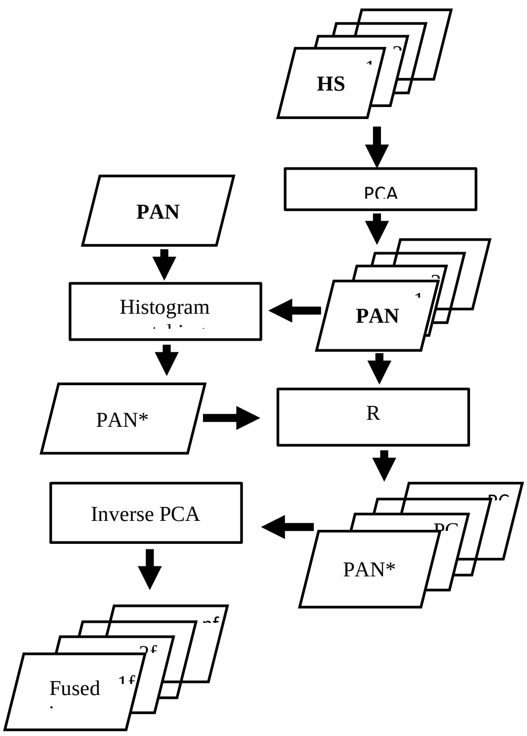


**Figure7. Schematic flow chart of PCA image fusion.**

## Performance Evaluation Measure

A variety of performance evaluation criteria, which can be divided into subjective and objective evaluation procedures, are available for assessing the effectiveness of various image fusion approaches. While the objective assessment of the fused image's quality is an unbiased process carried out by observers and greatly valued by visual perception (Seegers, *et al.*, 2018). In the absence of a reference image, fusing technique was compared quantitatively in this research using the following statistical measures.:

### Mean absolute error (MAE)

MAE is used to manipulate the fused image distortion degree. However, lower value of it indicates that the fused image as good quality (Seegers, *et al.*, 2018).

$$MAE = \frac{1}{MN}\sum_{i=1}^{M}\sum_{j=1}^{N}\left|G_{i,j} - \bar{G}_{i,j}\right| \quad ..(3)$$

$G_{i,j}$ represents the pixel value of the reference image G, and $\bar{G}_{i,j}$ is the pixel value of the fused image $\bar{G}$. M and N are the HR image sizes.

### Root Mean Square Error (RMSE)

RMSE represents the spatial and spectral distortion included in the fused image and offers the standard error of fused images (Mhangara, P., Mapurisa, W., and Mudau, N., 2020). It is expressed in Equation (4):

$$RMSE = \sqrt{\frac{1}{MN}\sum_{i=1}^{M}\sum_{j=1}^{N}\left(G_{i,j} - \bar{G}_{i,j}\right)^2} \quad .(4)$$

### Relative Dimensionless Global Error of Synthesis (ERGAS)

Erreur Relative Globale Adimensionalle de Synthèse (ERGAS) indices using the original hyperspectral and panchromatic band as a reference to assess the quality of the mixture with the following formula:

$$ERGAS = 100\ \frac{h}{l}\sqrt{\frac{1}{MN}\sum_{i=1}^{M}\sum_{j=1}^{N}\left(\frac{RMSE}{mean}\right)^2} \quad (5)$$

Where $h$ and $l$ are the resolutions of the PAN and HS images, respectively.

### Correlation Coefficient (CC)

CC refers to the correlation degree between the original image and pan-sharpened image. Its value Ranging between [−1,1]. So, one is the best value, which denoted to the highly correlated for compared images. However, A value of −1 means that one image is the

| a) PAN Image (15 m) | b) HS Image (30m) |
|---|---|

**Figure 8. a) PAN Image with spatial resolution (15 M) and b) HS image with spatial resolution (30 M).**

inverted version of the other (Zoran, 2009) Equation (6) describes how the CC is calculated:

$$CC = \frac{\sum_{i=1}^{M}\sum_{j=1}^{N}(\bar{\boldsymbol{G}}_{i,j}-\bar{\boldsymbol{m}})(G_{i,j}-\boldsymbol{m})^2}{\sqrt{\sum_{i=1}^{M}\sum_{j=1}^{N}(\bar{\boldsymbol{G}}_{i,j}-\bar{\boldsymbol{m}})^2(G_{i,j}-\boldsymbol{m})^2}} \quad \dots (6)$$

$m$, and $\bar{m}$ are the $G_{i,j}$ and the $\bar{G}_{i,j}$ mean respectively.

**Standard Deviation (STD)**

STD is used in fusion evaluation to measure contrast in the pan-sharpened image**.** It presents the discrete plane of the grayscale image's mean value. The fused image has a higher contrast when the sigma value is high, and vice versa. STD could define as follows: (Zoran, 2009)

$$STD = \sqrt{\sum_{i=1}^{M}\sum_{j=1}^{N}\frac{(G_{i,j}-\overline{Gray}_{i,j})^2}{MN}} \quad \dots (7)$$

$\overline{Gray}_{i,j}$, is the average gray value $G_{i,j}$

**Entropy (IE)**

IE is used for assessing the extent of information that fused image contains. The fused image has a rich information content if the entropy value is high: (Zoran, 2009)

$$IE = -\sum_{i=0}^{L-1} P_i \log P_i \quad \dots (8)$$

$L$ is the overall gray-scales of image, and $P_i$ is the probability of gray level *i*.

**Results and Discussion**

Improving the spatial resolution of high spectral resolution (HS) images is the goal of fusion technique. The basic images are shown in Figure 8. The Landsat 8 PAN image has a high spatial resolution (15 m) and was used to raise the spatial resolution of the HS images as shown in Figure 8.a. On the other hand, Figure 8.b represents the HS image from EO-1 satellite with spatial resolution (30m). The aim of the research is to increase the spatial resolution of all the hundreds of bands that consist HS images, each of which has a restricted spectral width of 10 nm. For this reason, a number of color combinations that are frequently used in some remote sensing applications such as the USGS (Simon, 2006) will be presented, which are shown in Figure 9. Figure 9.a represents the reference image according to the true color (RGB) model where the red (R), green (G), and blue (B) images correspond to the wavelengths of 640, 559, and 467nm, respectively, corresponding to HS bands (22, 14, 5). Figure 9.c represents the RGB color combination to provide a false color image from mixing three bands representing visible color and infrared (CIR) for the bands (43, 22, 14) that indicate NIR (854 nm), red (640 nm) and green. (559 nm), respectively. Figure 9.e represents the RGB color combination to

| | |
|---|---|
|  |  |
| a) Reference (RGB) =22, 14, 5 | b) Resultant (RGB) =22, 14, 5 |
|  |  |
| c) Reference (CIR)= 43, 22, 14 | d) Resultant (CIR)= 43, 22, 14 |
|  | 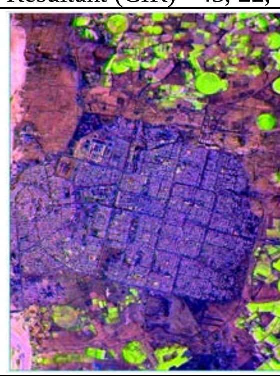 |
| e) Reference (SWIR1, NIR, R) = 115, 43, 22 | f) Resultant (SWIR1, NIR, R) = 115, 43, 22 |
|  |  |
| g) Reference (SWIR2, SWIR1, R) = 158, 115, 22 | h) Resultant (SWIR2, SWIR1, R) = 158, 115, 22 |

**Figure 9. (a, c, e and g) Reference images in four color combinations, (b, d, f and h) the results of the PC fusion method with the same color combinations**

provide a false color image for vegetation analysis by (SWIR1 band (115), NIR band (43), and red band (22)) which correspond to the wavelengths (1618 nm, 854 nm, 640 nm. Finally, Figure 9.g represents the RGB color combination to provide a false color image of the urban area represented by (SWIR2 band (158), SWIR1 band (115) and red band (22)) which correspond to wavelengths of (2193 nm, 1618 nm). and 640 nm), respectively.

The PC method is applied to fuse PAN image (Figure 8.a) with HS image (all 148 bands). The results of the fusion will be shown in Figure 9 in the same pattern of color combinations mentioned before, where (9.b) are true colors (RGB), (9. d) are false colors for visible colors and NIR colors (CIR), (9. f) in false colors for the vegetation analysis and (9. h) in false colors for the urban area. In order to visually discuss the fusion results, before and after fusing images. The purpose of changing the selection of color groups is to see the fusion effect on each component of the HS image.

The results demonstrated that using the PC fusion technique improves the scene's spatial resolution while maintaining the color components of HS images. as is clear from Figure 9. Subjective comparison is not enough because the eye cannot distinguish between small differences between complex details. However, the evaluation will be conducted using a number of quantitative criteria for four selected bands. Among the quantitative criteria MAE, RMSE, EGRAS, MAE-W, STD and IE, which were applied to the results of the PC fusion technique as shown in Table 3.

**Table 4. Quantitative evaluation of PC fusion results.**

| *Fusion* | | *a)* | *With HS original Reference* | | | *b)* | *Without Reference* |
|---|---|---|---|---|---|---|---|
| *Bands* | *MAE* | *RMSE* | *ERGAS* | *CC* | *MAE-W* | *STD* | *IE* |
| *Blue* | **0.212** | **0.232** | **20.018** | **0.626** | **0.083** | **0.102** | **6.729** |
| *Green* | **0.140** | **0.171** | **16.465** | **0.026** | **0.057** | **0.074** | **6.237** |
| *Red* | **0.206** | **0.239** | **19.399** | **0.097** | **0.061** | **0.080** | **6.361** |
| *AVG* | **0.186** | **0.214** | **18.627** | **0.250** | **0.067** | **0.085** | **6.442** |

The ideal values for MAE, RMSE and EGRAS are zero, and the smaller the values of these parameters indicate better fusion results, and this is consistent with the results published by Loncan in 2016 (Loncan, *et al.*, 2015).

The results showed that the values of the quantitative variables (MAE, RMSE, EGRAS), calculated relative to the reference HS image are low and vary from one band to another. Differences in these errors depending on the band can be attributed to the difference in the spectral response of these bands. The MAE calculated in the presence and absence of the reference, where a smaller (better) value without the reference indicates richer information in the merged image. The correlation coefficient (CC) varies significantly by band as well, with the highest CC value (0.626) recorded for the blue band. A higher CC value means better results.

## Conclusion

The adoption of image fusion techniques in this research regards the most effective image processing strategies to maximize the potential of HS image according to its significant importance in remote sensing.

This technique has been applied on preprocessed HS image and PAN obtained fused HS image with 15m spatial resolution and 148 bands. This leads to results in a wider use of the broad spectrum in it, especially for the study area, where the buildings were more distinct inside the urban area and the vegetation regions became simpler to study. This leads to a greater use of these images.

## Recommendation

- Future studies might focus on the research results to use in all remote sensing fields due to its unique characteristic.
- Research on the results spectral analyzes and comparing them with spectral libraries, considering that the image contains a large number of bands with a resolution of 15 meters.
- Adopting methods for fusion HS image from Hyperion sensor with PAN image from Advanced Land Imager (ALI) sensor. which they both belong to the EO-1, and comparing the results with ours.

## References

**Aiazzi**, B., Baronti, S., and Selva, M. (2007). Improving component substitution pansharpening through multivariate regression of MS $+ $ Pan data. *IEEE Transactions on Geoscience and Remote Sensing, 45*(10), pp. 3230-3239.

**Awad**, M. (2018). Forest mapping: a comparison between hyperspectral and multispectral images and technologies. *Journal of Forestry Research*, 29, (5), pp. 1395-1405.

**Barry**, P. (2001). EO-1/Hyperion science data user's guide, Level 1_B. *RW Space, Defense & Information Systems, Redondo Beach, CA, Rep. HYP. TO, 1*.

**Beck**, R. (2003). *EO-1 User Guide-Version 2.3.* Satellite Systems Branch, USGS Earth Resources Observation Systems Data Center (EDC) .

**Camacho**, A., Vargas, E., and Arguello, H. (2022). Hyperspectral and multispectral image fusion addressing spectral variability by an augmented linear mixing model. *International Journal of Remote Sensing, 43*(5), pp. 1577-1608.

**Griffin**, M.K., and Burke, H.-h.K. (2003). Compensation of hyperspectral data for atmospheric effects. *Lincoln Laboratory Journal, 14*(1), pp. 29-54.

**Guo**, H., Bao, W., Qu, K., Ma, X., and Cao, M. (2022). Multispectral and hyperspectral image fusion based on regularized coupled non-negative block-term tensor decomposition. *Remote Sensing, 14*(21), pp. 5306.

**Imani**, M., and Ghassemian, H. (2020). An overview on spectral and spatial information fusion for hyperspectral image classification: Current trends and challenges. *Information fusion, 59*, pp. 59-83.

**Jagalingam** Pa, A. (2015). A Review of Quality Metrics for Fused Image. *ScienceDirect, Elsevier, 4*, pp. 133-142.

**Jasim**, Y.A., Al-Ani, A.A., and Al-Ani, L.A. (2018). Iris recognition using principal component analysis. In *Book Iris recognition using principal component analysis* (pp. pp. 89-95). (IEEE, 2018, edn.): in Editor (Ed.)^(Eds.): ‘’ (IEEE, 2018, edn.), .

**Lodhi**, V., Chakravarty, D., and Mitra, P. (2018). Hyperspectral imaging for earth observation: Platforms and instruments. *Journal of the Indian Institute of Science*, 98, pp. 429-443.

**Loncan**, L., De Almeida, L.B., Bioucas-Dias, J.M., Briottet, X., Chanussot, J., Dobigeon, N., Fabre, S., Liao, W., Licciardi, G.A., and Simoes, M. (2015). Hyperspectral pansharpening: A review. *IEEE Geoscience and remote sensing magazine, 3*(3), pp. 27-46.

**Mhangara**, P., Mapurisa, W., and Mudau, N. (2020). Comparison of image fusion techniques using satellite pour l’Observation de la Terre (SPOT) 6 satellite imagery. *Applied Sciences, 10*(5), pp. 1881.

**Plaza**, A., Benediktsson, J.A., Boardman, J.W., Brazile, J., Bruzzone, L., Camps-Valls, G., Chanussot, J., Fauvel, M., Gamba, P., and Gualtieri, A. (2009). Recent advances in techniques for hyperspectral image processing. *Remote sensing of environment, 113*, pp. S110-S122.

**Rawnak-a-** A. Abdulwahab, et al. (2023). Hyperspectral Pansharpening Improvement using MNF Transformation. *AIP Conf. Proc., 3018*(020052).

**Rawnak-b-** A. Abdulwahab, et al. (2023). Fused Images Based on Division of Hyperspectral Images into Spectral Groups. *AIP Conf. Proc., 3018*(020009 ).

**Saadallah**, M. A. (2023). *LAND COVER CHANGES USING PRINCIPAL COMPONENT ANALYSIS OF MULTI TEMPORAL SATELLITE IMAGES PAIRS.* Bagdad: Al-nahrain university.

**Seegers**, B.N., Stumpf, R.P., Schaeffer, B.A., Loftin, K.A., and Werdell, P.J. (2018). Performance metrics for the assessment of satellite data products: an ocean color case study. *Optics express, 26*(6), pp. 7404-7422.

**Selva**, M., Aiazzi, B., Butera, F., Chiarantini, L., and Baronti, S. (2015). Hyper-sharpening: A first approach on SIM-GA data. *IEEE Journal of selected topics in applied earth observations and remote sensing, 8*(6), pp. 3008-3024.

**Shabin** Muhammed, R.D., Vishnukumar S. (2020). Hyperspectral and Multispectral Image Fusion. *International Journal of Recent Technology and Engineering (IJRTE), 8*(5), pp. 467-471.

**Shimal**, M.S., and Shaban, A.H. (2020). Evaluation of the Pollution Elements at

Samara Water Table–Iraq. *Iraqi Journal of Science*, *61*(4), pp. 898-907.

**Simon**, K. (2006). *Hyperion Level 1GST (L1GST) Product Output Files Data Format Control Book (DFCB): Earth Observing-1 (EO-1)(No. Version 1.0).* Sioux Falls: United States Geological Survey.

**un**, W., Chen, B., and Messinger, D.W. (2014). Nearest-neighbor diffusion-based pan-sharpening algorithm for spectral images. *Optical Engineering*, *53*(1), pp. 013107-013107.

**Wang**, W., and Chang, F. (2011). A Multi-focus Image Fusion Method Based on Laplacian Pyramid. *J. Comput.*, *6*(12), pp. 2559-2566.

**Ying**, J., Shen, H.-L., and Cao, S.-Y. (2021). Unaligned hyperspectral image fusion via registration and interpolation modeling. *IEEE Transactions on Geoscience and Remote Sensing*, *60*, pp. 1-14.

**Zoran**, L. (2009). Quality evaluation of multiresolution remote sensing images fusion. *UPB Sci Bull Series C*, *1*, 71.